Transition states for psychrophilic and mesophilic (*R*)-3-hydroxybutyrate dehydrogenase-catalysed hydride transfer at sub-zero temperature

Teresa F. G. Machado,[†] Miha Purg,[§] Johan Åqvist,[§] and Rafael G. da Silva[‡,*]

[†]School of Chemistry, Biomedical Sciences Research Complex, University of St Andrews, St Andrews, Fife KY16 9ST, United Kingdom

[‡]School of Biology, Biomedical Sciences Research Complex, University of St Andrews, St Andrews, Fife KY16 9ST, United Kingdom

[§]Department of Cell and Molecular Biology, Biomedical Center, Uppsala University, Box 596, SE-751 24, Uppsala, Sweden

*To whom correspondence may be addressed: rgds@st-andrews.ac.uk, phone: +44 01334 463496

Abstract. (*R*)-3-hydroxybutyrate dehydrogenase (HBDH) catalyses the NADH-dependent reduction of 3-oxocarboxylates to (*R*)-3-hydroxycarboxylates. The active sites of a pair cold- and warm-adapted HBDHs are identical except for a single residue, yet kinetics evaluated at −5, 0, and 5 °C show much higher steady-state rate constant (k_{cat}) for the cold-adapted than for the warm-adapted HBDH. Intriguingly, single-turnover rate constants (k_{STO}) are strikingly similar between the two orthologues. Psychrophilic HBDH primary deuterium kinetic isotope effects on k_{cat} ($^{D}k_{cat}$) and k_{STO} ($^{D}k_{STO}$) decrease at lower temperature, suggesting more efficient hydride transfer relative to other steps as temperature decreases. However, mesophilic HBDH $^{D}k_{cat}$ and $^{D}k_{STO}$ are generally temperature-independent. The $^{D}k_{STO}$ data allowed calculation of intrinsic primary deuterium kinetic isotope effects. Intrinsic isotope effects of 4.2 and 3.9 for cold- and warm-adapted HBDH, respectively, at 5 °C, supported by QM/MM calculations, point to a late transition state for both orthologues. Conversely, intrinsic isotope effects of 5.7 and 3.1 for cold- and warm-adapted HBDH, respectively, at −5 °C indicate the transition state becomes nearly symmetric for the psychrophilic enzyme, but more asymmetric for the mesophilic. His-to-Asn and Asn-to-His mutations in the psychrophilic and mesophilic HBDH active sites, respectively, swap the single active-site position where these orthologues diverge. At 5 °C, the His-to-Asn mutation in psychrophilic HBDH decreases $^{D}k_{cat}$ to 3.1, suggesting a decrease in transition-state symmetry, while the His-to-Asn mutation in mesophilic HBDH increases $^{D}k_{cat}$ to 4.4, indicating an increase in transition-state symmetry. Hence, temperature adaptation and a single divergent active-site residue may influence transition-state geometry in HBDHs.

Keywords: 3-hydroxybutyrate dehydrogenase, kinetic isotope effects, low-temperature catalysis, hydride transfer, transition-state structure

INTRODUCTION

Short-chain dehydrogenases/reductases (SDR) are ubiquitous across all domains of life and constitute one of the largest known protein superfamilies.[1] Key features of SDR enzymes include a conserved tertiary structure and a strictly conserved Ser-Tyr-Lys catalytic triad, but low overall amino acid sequence identity.[2] Due to their high enantioselectivity, natural and engineered SDRs are useful biocatalysts in asymmetric carbonyl reductions to produce chiral alcohols.[3, 4] (*R*)-3-hydroxybutyrate dehydrogenase (HBDH) (EC 1.1.1.30) is an SDR that catalyses the reduced nicotinamide-adenine dinucleotide (NADH)-dependent reduction of acetoacetate to (*R*)-3-hydroxyburyrate (Scheme 1).[5] HBDH also catalyses the reduction of 3-oxovalerate, albeit drastically more slowly.[5] The products of the HBDH reaction, (*R*)-3-hydroxycarboxylates, are chiral precursors in the synthesis of value-added compounds such as antibiotics,[6] and also form the monomeric units of biodegradable polyesters.[7] Thus, recent attempts have been made to harness the catalytic properties of HBDH towards the production of its native and non-native products via biocatalysis and synthetic biology.[8-10]

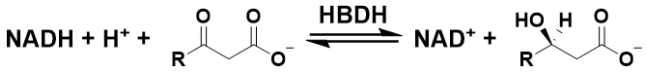

R = CH_3: Acetoacetate and (*R*)-3-hydroxybutyrate
R = CH_2CH_3: 3-Oxovalerate and (*R*)-3-hydroxyvalerate

Scheme 1. HBDH-catalysed reaction.

We have recently established the temperature-rate profiles of a psychrophilic (from *Psychrobacter arcticus*) and a mesophilic (from *Acinetobacter baumannii*) HBDH.[11] *P. arcticus* and *A. baumannii* are members of the bacterial family *Moraxellaceae*, but the former is an extreme psychrophile from the arctic permafrost growing at temperatures constantly below 0 °C,[12] while the latter is a mesophilic human pathogen that grows at 37 °C.[13] We observed much higher catalytic rates for *P. arcticus* HBDH (*Pa*HBDH) than for *A. baumannii* HBDH (*Ab*HBDH) throughout the experimental temperature range,[11] a common trend

observed in comparative studies of psychrophilic and mesophilic enzymes.[14] Surprisingly, *Pa*HBDH has a melting temperature (T_m) of 57 °C, which increases to 64 °C in the presence of the NADH.[11] The combination of high catalytic rate and thermostability[4] makes *Pa*HBDH a promising biocatalyst for the synthesis of (*R*)-3-hydroxycarboxylates.

We have also used deuterium kinetic isotope effects, protein crystallography and quantum mechanics/molecular mechanics (QM/MM) calculations to demonstrate that *Pa*HBDH and *Ab*HBDH catalysis proceeds via concerted hydride and proton transfers.[15] Additionally, both enzymes show a highly conserved active site with a single diverging residue: *Pa*HBDH His150 is equivalent to Asn145 in *Ab*HBDH. The mutant Asn145His-*Ab*HBDH has only modestly decreased rate in comparison with the wild-type (WT) enzyme, but His150Asn-*Pa*HBDH displays drastically reduced catalysis in comparison with WT-*Pa*HBDH.[15] Nevertheless, these kinetic studies were carried out at 10 °C,[15] a significantly higher temperature than the −10 to −5 °C of the natural environment of *P. arcticus*.[12]

In the present work we employ primary deuterium kinetic isotope effects under steady-state and single-turnover conditions at −5, 0, and 5 °C to determine rate-limiting steps and transition-state structures of the reaction catalysed by *Pa*HBDH and *Ab*HBDH near the temperature of *P. arcticus*'s natural environment. We also establish the effect His150/Asn145 may exert on transition-state symmetry. Elucidation of the intricacies of HBDH catalysis may aid future engineering efforts of this enzyme.

MATERIALS AND METHODS

Materials. All commercially available chemicals were used without further purification. Reduced nicotinamide adenine dinucleotide (NADH), oxidised nicotinamide adenine dinucleotide (NAD^+), D-glucose, *Pseudomonas* sp**.** glucose dehydrogenase, and acetoacetate were purchased from Sigma-Aldrich. Deuterium-labelled D-glucose (1-D, 98%)

was purchased from Cambridge Isotope Laboratories, and 3-oxovalerate was purchased from Carbosynth. NADH and 4*S*-[4-^{2}H]NADH (NADD) were synthesised and purified as previously described.[15] *Pa*HBDH, *Ab*HBDH, His150Asn-*Pa*HBDH, His150Ala-*Pa*HBDH, Asn145His-*Ab*HBDH and Asn145Ala-*Ab*HBDH were expressed and purified as previously described.[11, 15]

***Pa*HBDH and *Ab*HBDH saturation kinetics in the presence of methanol.** *Pa*HBDH (5 nM) initial rates were measured at 10 °C in the presence of 0% and 10% methanol (*v/v*) at varying concentrations of one substrate, either acetoacetate (0.025 – 0.4 mM) or NADH (0.01 – 0.160 mM), and a fixed, saturating concentration of the other (either 0.4 mM acetoacetate or 0.160 mM NADH). *Ab*HBDH (50 nM) initial rates were measured at 10 °C in the presence of 0% and 10% methanol (*v/v*), varying concentrations of one substrate, either acetoacetate (0.05 – 0.8 mM) or NADH (0.02 – 0.32 mM), and a fixed, saturating concentration of the other (either 0.8 mM acetoacetate or 0.32 mM NADH). All measurements were performed at least in duplicate in a Shimadzu UV-2600 spectrophotometer by monitoring the decrease in absorbance at 340 nm ($\varepsilon = 6220\ M^{-1}\ cm^{-1}$) due to the oxidation of NADH, in 1-cm optical path length quartz cuvettes (Hellma).

***Pa*HBDH and *Ab*HBDH steady-state kinetic isotope effects.** Primary deuterium kinetic isotope effects on the steady-state catalytic rate constant ($^{D}k_{cat}$) were determined using NADH or NADD to reduce either acetoacetate or 3-oxovalerate in 100 mM HEPES, pH 7.0 at −5, 0, and 5 °C in the presence of 10% methanol (*v/v*) by measuring initial rates in the presence of saturating concentrations of both substrates (*Pa*HBDH: 0.2 – 0.4 mM acetoacetate, 0.04 mM NADH and 0.02 mM NADD, 10 nM *Pa*HBDH; 0.4 – 0.8 mM 3-oxovalerate, 0.005 NADH, 0.2 – 0.4 mM 3-oxovalerate, 0.005 NADD, 30 nM *Pa*HBDH; *Ab*HBDH: 0.8 – 1.6 mM acetoacetate, 0.32 mM NADH or 0.16 mM NADD, 100 nM *Ab*HBDH; 0.4 – 0.8 mM 3-

oxovalerate, 0.16 mM NADH or NADD, 1 μM *Ab*HBDH). Kinetic isotope effects were calculated by dividing the k_{cat} values obtained with NADH by the corresponding values obtained with NADD at the higher substrate concentration. All reactions were monitored at 340 nm in an Applied Photophysics SX-20 stopped-flow spectrophotometer outfitted with a xenon lamp, a 5-μL mixing cell (0.5-cm path length and 0.9-ms dead-time) and a circulating water bath for temperature control. One syringe contained enzyme and the other, the substrates. Both syringes contained buffer and methanol. Reactions were triggered by rapidly mixing 55 μL from each syringe and monitored for 60 s. A minimum of 5 traces with 10000 data-points per trace were collected for each concentration at each temperature.

Single-turnover kinetic isotope effects. All reactions were carried out in 100 mM HEPES (pH 7.0) and 10% methanol (*v/v*) at −5, 0 and 5 °C by monitoring the decrease in absorbance at 340 nm due to consumption of either NADH or NADD in an Applied Photophysics SX-20 stopped-flow spectrophotometer. Single-turnover rates for *Pa*HBDH were measured at saturating concentrations of 3-oxovalerate (1.1 mM or 0.336 mM when either NADH or NADD were used, respectively), 4 μM NADH or NADD, and enzyme concentrations of 40 μM and 50 μM. *Pa*HBDH and either NADH or NADD was kept in one syringe and 3-oxovalerate in another. For *Ab*HBDH, single-turnover rates were measured at saturating concentrations of 3-oxovalerate (3.45 mM and 3 mM when either NADH or NADD were used, respectively), 4 μM NADH or NADD, and enzyme concentrations of 40 μM and 50 μM. *Ab*HBDH and either NADH or NADD were kept in one syringe and 3-oxovalerate in another. Reaction was triggered by rapidly mixing 55 μL from each syringe. A minimum of 6 traces with 10000 data-points per trace were collected for each enzyme concentration at each temperature. Primary deuterium kinetic isotope effects on the single-turnover rate constant ($^{D}k_{STO}$) were calculated as the ratio between the k_{STO} with NADH to that with NADD at the higher enzyme concentration.

***Pa*HBDH and *Ab*HBDH mutants steady-state kinetic isotope effects.** Initial rates of acetoacetate reduction catalysed by HBDH mutants were measured at 5 °C with either NADH or NADD, under the same conditions as for the WT-HBDHs in the presence of saturation concentrations of acetoacetate and coenzyme. For His150Ala-*Pa*HBDH: 5.4 - 10.8 mM acetoacetate, 0.032 mM NADH or NADD; 0.016 – 0.032 mM NADH, 10.8 mM acetoacetate; and 0.032 mM NADD, 10.8 mM acetoacetate; 0.4 μM enzyme. For Asn145Ala-*Ab*HBDH: 5.4 – 10.8 mM acetoacetate, 0.04 mM NADH or NADD; 0.02 – 0.04 mM NADH, 10.8 mM acetoacetate; 0.04 mM NADD, 10.8 mM acetoacetate; 1.5 μM enzyme. For His150Asn-*Pa*HBDH: 21.6 mM acetoacetate, 0.08 mM NADH or NADD; 7 μM enzyme. For Asn145His-*Ab*HBDH: 10.8 – 21.6 mM acetoacetate, 0.08 mM NADH or NADD; 0.04 – 0.08 mM NADH, 21.6 mM acetoacetate; and 0.08 mM NADD, 21.6 mM NADD, 0.4 μM enzyme. All reactions were monitored at 340 nm in an Applied Photophysics SX-20 stopped-flow spectrophotometer. One syringe contained enzyme and the other, the substrates. Both syringes contained buffer and methanol. Reactions were triggered by rapidly mixing 55 μL from each syringe and monitored for 60 s. A minimum of 4 traces with 5000 data-points per trace were collected for each concentration with exception of His150Asn-*Pa*HBDH where 3 traces were collected.

Kinetic data analysis. Kinetic data were analysed by the nonlinear regression function of SigmaPlot 14 (SPSS Inc.). Data points and error bars in graphs represent mean ± standard error of independent measurements, and kinetic and equilibrium constants are presented as mean ± fitting error, unless otherwise stated.

Substrate saturation curves were fitted to eq 1 where v is the initial rate, E_T is total enzyme concentration, S is the concentration of the varying substrate, k_{cat} is the steady-state catalytic constant, and K_M is the Michaelis constant.

$$\frac{v}{E_T} = \frac{k_{cat}S}{K_M+S} \qquad \text{eq 1}$$

Pre-steady-state single-turnover data were fitted to eq 2, where $[NADH]_t$ is the concentration of NADH at time t, $[NADH]_\infty$ is the NADH concentration as time approaches infinite, A_0 is the amplitude change, t is the reaction time, and k_{STO} is the single-turnover rate constant.

$$[NADH]_t = [NADH]_\infty + A_0 e^{-k_{STO}t} \qquad \text{eq 2}$$

Time-dependent kinetic isotope effects. Time-dependent kinetic isotope effects (tKIEs) for *Pa*HBDH- and *Ab*HBDH-catalysed reduction of 3-oxovalerate were extracted from the pre-steady-state single-turnover kinetics data by the method of Palfey and Fagan.[16] The derivatives were calculated by dividing the change in consecutive NADH(D) concentrations by the corresponding change in time from the lines of best fit of the single-turnover data to eq 2, with the tKIEs calculated from these derivatives via eq 5 (see Results and Discussion) where numerator and denominator were the mean ± SE from at least 6 best fit lines (each from an individual reaction trace). The intrinsic primary deuterium kinetic isotope effect ($^{D}k_5$) was taken from the tKIE value at $t = 0$. This process was carried out for single-turnover data collected at −5, 0 and 5 °C.

Computation of theoretical isotope effects. Ground-state and transition-state structures for *Pa*HBDH- and *Ab*HBDH-catalysed reduction of 3-oxovalerate were calculated via QM/MM at M06-2X/ma-def2-SVP level of theory using ORCA 4.2.1 exactly as previously reported.[15] Briefly, employing a micro/macro-iteration strategy (micro: M02-2X/ma-def2-SVP//CHARMM; macro: GFN-XTB2//CHARMM) we further optimized and characterized the reactant, product and transition state stationary points. All calculations were performed in 10 replicates, for which the initial structures were collected as equidistance snapshots from a

10-ns classical molecular dynamics simulation at 293 K. Kinetic isotope effects were calculated using the semi-classical transition-state theory approach, employing the Bigeleisen-Mayer equation for calculating vibrational contributions, and using the one-dimensional Bell infinite parabola correction for tunneling as implemented in Kinisot.[17] The modifications to Kinisot for reading ORCA hessians are readily available at https://github.com/mpurg/kinisot. QM/MM hessians of reactant and transition states from our previous study were mass-weighted and diagonalized to obtain harmonic vibrational frequencies and Bigeleisen-Mayer reduced isotopic partition function ratios. The lowest 6 vibrational modes (translational and rotational degrees of freedom) were discarded. A scaling factor of 0.9795 was used.[18] KIEs were computed independently for each of the 10 sets of reactant and transition states from the QM/MM calculations referred to above. Individual contributions to the semi-classical KIEs as well as the Bell correction for tunneling were calculated at −5, 0, and 5 °C. Final values are arithmetic means of tunneling-corrected KIEs over all 10 replicates for each ortholog at each temperature. The individual contributions to the KIE for each of the 10 replicates for *Pa*HBDH and *Ab*HBDH are shown in Tables S1 and S2, respectively.

RESULTS AND DISCUSSION

Low-temperature primary deuterium kinetic isotope effects on k_{cat}. To probe the hydride-transfer step near the environmental temperature of *Pa*HBDH, k_{cat} was determined with both enzymes for acetoacetate and 3-oxovalerate reduction at −5, 0 and 5 °C in the presence of either NADH or NADD (Figure 1) using a stopped-flow spectrophotometer. To prevent solution freezing at 0 and −5 °C, reactions at all three temperatures were carried out in the presence of 10% methanol (*v/v*), which was shown to have only a very small effect on the reaction by comparing the kinetics of acetoacetate reduction in the presence and absence of methanol at 10 °C (Figure S1). The highest difference observed was a 7% reduction in k_{cat} for

*Pa*HBDH in the presence of methanol, which is negligible in comparison with all isotope effects measured here (see below). Saturating concentrations of all substrates were used, and rate constants were confirmed to be unimolecular by their insensitivity to a lower concentration of substrates (Figure S2).

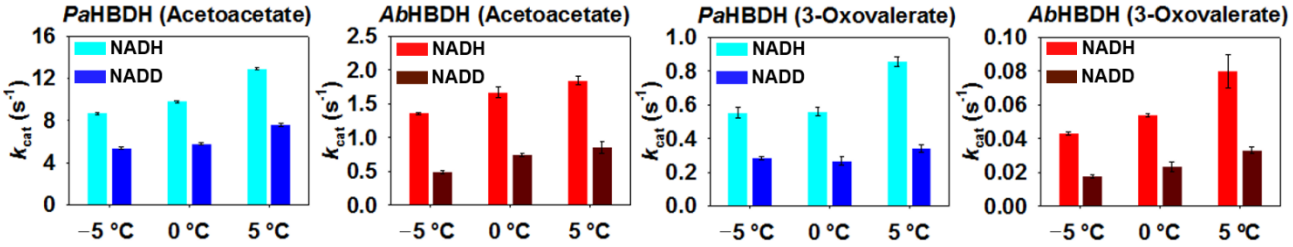

Figure 1. *Pa*HBDH and *Ab*HBDH k_{cat} for acetoacetate and 3-oxovalerate reduction at −5, 0 and 5 °C in the presence of either NADH or NADD. All substrates and coenzymes were held at saturating concentrations. Each bar represents mean ± SE of at least five replicates.

The k_{cat} values for NADH-dependent reduction, summarised in Table S3, reflect the distinct temperature adaptations of the enzymes, with k_{cat} 5- to 7-fold higher for *Pa*HBDH than for *Ab*HBDH for acetoacetate reduction, and 10- to 12-fold higher for the psychrophilic orthologue than for the mesophilic one for 3-oxovalerate reduction. The k_{cat} observed for *Pa*HBDH between −5 and 5 °C follow the same trend described at higher temperatures where the values with 3-oxovalerate are ~15-fold lower than with acetoacetate.[11] In contrast, *Ab*HBDH k_{cat} with 3-oxovalerate at −5 and 0 °C are 31-fold lower than with acetoacetate, far from the 11- to 22-fold difference at higher temperatures,[11] showing the challenge of catalysis with the non-native substrate is disproportionately compounded at very low temperature.

The data displayed in Figure 1 were utilised to calculate $^{D}k_{cat}$ (Table 1). For acetoacetate reduction, *Pa*HBDH $^{D}k_{cat}$ is modest and temperature-independent, while *Ab*HBDH $^{D}k_{cat}$ modestly increases from 2.2 at 5 °C, the same value found at 10 °C,[15] to 2.8 at −5 °C. This points to chemistry remaining faster than other steps at low temperature for *Pa*HBDH, but

becoming more rate-limiting for *Ab*HBDH at lower temperature. For 3-oxovalerate reduction, *Ab*HBDH $^{D}k_{cat}$ is significant and temperature-independent. However, *Pa*HBDH $^{D}k_{cat}$ decreases from 2.5 at 5 °C to 1.9 at −5 °C, indicating that hydride transfer to 3-oxovalerate is less rate-limiting at sub-zero temperature.

Table 1. Primary deuterium kinetic isotope effects on k_{cat} ($^{D}k_{cat}$) for *Pa*HBDH- and *Ab*HBDH-catalysed reduction of acetoacetate and 3-oxovalerate.

Enzyme substrate	−5 °C	0 °C	5 °C
***Pa*HBDH acetoacetate**	1.63 ± 0.02	1.69 ± 0.03	1.70 ± 0.04
***Ab*HBDH acetoacetate**	2.8 ± 0.2	2.3 ± 0.1	2.2 ± 0.1
***Pa*HBDH 3-oxovalerate**	1.9 ± 0.1	2.1 ± 0.2	2.5 ± 0.2
***Ab*HBDH 3-oxovalerate**	2.4 ± 0.1	2.3 ± 0.3	2.5 ± 0.2

Low-temperature primary deuterium kinetic isotope effects on k_{STO}. In an attempt to eliminate some of the kinetic complexity inherent to k_{cat} and possibly unmask the expression of the primary deuterium kinetic isotope effects at low temperature, *Pa*HBDH and *Ab*HBDH k_{STO} were determined for 3-oxovalerate reduction in the presence of either NADH or NADD as the limiting reagent and saturating enzyme concentration (Figure 2). Reduction of 3-oxovalerate was chosen because both enzymes already displayed sizable $^{D}k_{cat}$ with this substrate. All k_{STO} were largely independent of enzyme concentration, since a 20% reduction in enzyme concentration caused either no difference or in some cases only very small differences in k_{STO} (Figure S3), suggesting NADH and NADD are saturated with enzyme and k_{STO} is unimolecular.[19] With NADH as coenzyme, *Pa*HBDH k_{STO} are 2- to 3-fold higher than the corresponding k_{cat}, while *Ab*HBDH k_{STO} are 19- to 26-fold higher than the corresponding k_{cat}. The large k_{STO}/k_{cat} ratio for *Ab*HBDH is intriguing given the significant $^{D}k_{cat}$ obtained for

this enzyme (Table 1). Nevertheless, the most remarkable result is the similarity between *Pa*HBDH and *Ab*HBDH k_{STO} at low temperature (Figure 2). This means the interconversion between HBDH:NADH:3OV and HBDH:NAD^+:3HV complexes described by k_{STO}, which encompasses the chemical step, does not reflect the distinct temperature adaptation of the two enzymes as k_{cat} does.

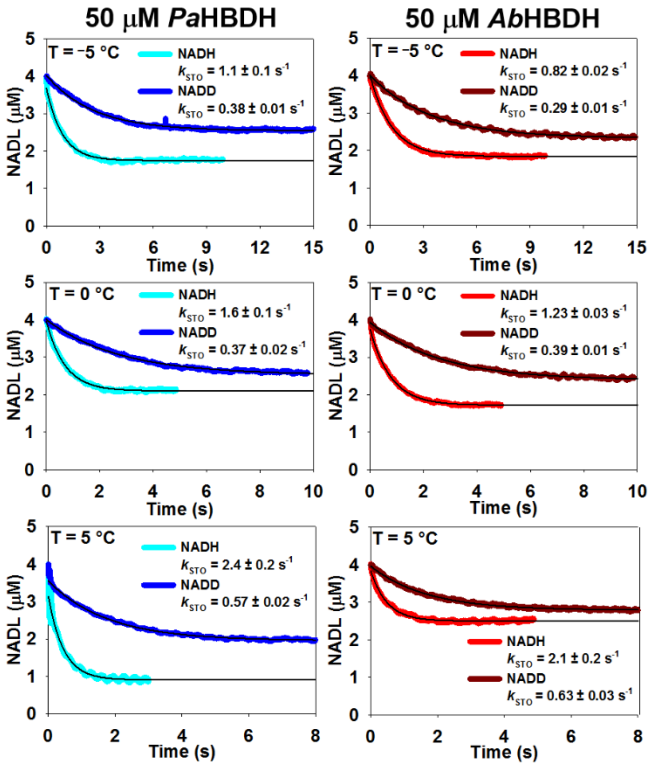

Figure 2. *Pa*HBDH and *Ab*HBDH k_{STO} for 3-oxovalerate reduction at −5, 0 and 5 °C in the presence of either NADH or NADD. Enzyme concentration is 50 μM, and NADL (where L denotes either H or D) concentration is 4 μM. Values represent mean ± SE of at least 6 replicates. Lines of best fit to eq 2 are in black.

All $^{D}k_{STO}$ (Table 2) increased in comparison with the corresponding $^{D}k_{cat}$ (Table 1), with *Pa*HBDH reflecting the most significant changes. *Pa*HBDH $^{D}k_{STO}$ decreases from 4.2 at 5 °C to 2.9 at −5 °C, while *Ab*HBDH $^{D}k_{STO}$ is less temperature-dependent, with only a modest decrease between 5 °C and −5 °C. These trends are in agreement with those found for $^{D}k_{cat}$, and

reinforce the hypothesis that *Pa*HBDH-catalysed hydride transfer to 3-oxovalerate is less rate-limiting at −5 °C than at 5 °C, whereas *Ab*HBDH-catalysed hydride transfer to 3-oxovalerate has comparable contribution to the rate-limiting step at all three temperatures.

Table 2. Primary deuterium kinetic isotope effects on k_{STO} ($^{D}k_{STO}$) for *Pa*HBDH- and *Ab*HBDH-catalysed reduction of 3-oxovalerate.

	–5 °C	**0 °C**	**5 °C**
***Pa*HBDH** $^{D}k_{STO}^{3OV}$	2.9 ± 0.4	4.3 ± 0.2	4.2 ± 0.2
***Ab*HBDH** $^{D}k_{STO}^{3OV}$	2.8 ± 0.1	3.2 ± 0.1	3.3 ± 0.2

Intrinsic primary deuterium kinetic isotope effects. In most enzymatic reactions, several isotope-insensitive steps contribute to the overall reaction rate, masking the expression of the intrinsic isotope effect, *i. e.* the isotope effect one would measure were chemistry fully rate-determining.[20, 21] Nevertheless, the intrinsic isotope effect is the only one that reflects the true differences in vibrational frequencies between reactant and transition states. Hence, for enzymatic transition-state geometry to be gleaned from isotope effects, their intrinsic values must be extracted from observed ones.[22, 23]

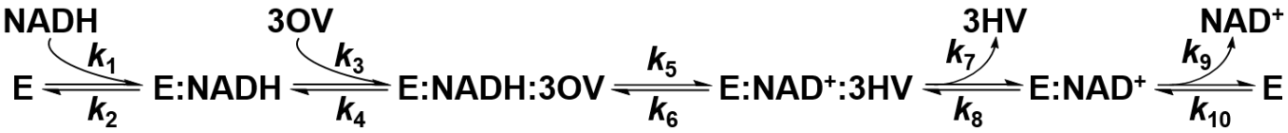

Scheme 2. Kinetic mechanism for reduction of 3-oxovalerate (3OV) to (*R*)-3-hydroxyvalerate (3HV) by *Pa*HBDH and *Ab*HBDH.

HBDH reaction follows an ordered kinetic mechanism where NADH is the first to bind to the free enzyme (Scheme 2).[15, 24, 25] The single-turnover experiment described above was designed to ensure pseudo-first-order conditions, with the interconversion between ternary

complexes describing a unimolecular process ($k_{STO} = k_5 + k_6$), and using the same concentrations of NADH and NADD (assuming they have the same extinction coefficient at 340 nm). This is an ideal system to apply the method of Palfey and Fagan for extraction of intrinsic isotope effects from pre-steady-state data,[16] a general expansion of the theory developed by Maniscalco *et al.*,[26] whose theoretical basis proves that the limit of the tKIE as *t* approaches 0 equals the intrinsic kinetic isotope effect.

Provided any potential equilibrium binding isotope effect falls within the expected uncertainty range of the experimental data, the intrinsic kinetic isotope effect ($^{D}k_5$) is given by eq 3, where k_5^{H} and k_5^{D} are the forward rate constants for the reactions with NADH and NADD, respectively. Solving for k_5^{D} yields eq 4. The tKIE for this reaction is obtained from eq 5, and the differential equation describing the system is given by eq 6. The limit of the tKIE as *t* approaches 0 is given by eq 7, which yields $^{D}k_5$ by noting that [E:NAD$^+$:3HV] = 0 at $t = 0$ and [E:NADH:3OV] = [E:NADD:3OV] at $t = 0$.

$$^{D}k_5 = \frac{k_5^H}{k_5^D} \qquad \text{eq 3}$$

$$k_5^D = \frac{k_5^H}{^{D}k_5} \qquad \text{eq 4}$$

$$tKIE = \frac{-\frac{d[E:NADH:3OV]}{dt}}{-\frac{d[E:NADD:3OV]}{dt}} \qquad \text{eq 5}$$

$$tKIE = \frac{k_5^H[E:NADH:3OV] - k_6^H[E:NAD^+:3HV]}{\frac{k_5^H}{^{D}k_5}[E:NADD:3OV] - k_6^D[E:NAD^+:3HV]} \qquad \text{eq 6}$$

$$\lim_{t\to 0} tKIE = \lim_{t\to 0} \frac{k_5^H[E:NADH:3OV]}{\frac{k_5^H}{^{D}k_5}[E:NADD:3OV]} = \frac{k_5^H}{\frac{k_5^H}{^{D}k_5}} = {}^{D}k_5 \qquad \text{eq 7}$$

Applying this method to the single-turnover kinetics data for 3-oxovalerate reduction

yields the tKIEs depicted in Figure 3, and the $^{D}k_5$ summarised in Table 3. For *Pa*HBDH, $^{D}k_5$ equals $^{D}k_{STO}$ at 5 °C (Tables 2 and 3), establishing that at this temperature, hydride transfer is rate-determining for conversion of *Pa*HBDH:NADH:3OV to *Pa*HBDH:NAD^+:3HV. However, $^{D}k_5 > {}^{D}k_{STO}$ at −5 °C (Tables 2 and 3), confirming hydride transfer is only partially rate-limiting, and an isotope-insensitive step, possibly a conformational change, must significant influence the rate. For *Ab*HBDH, on the other hand, $^{D}k_5 \sim {}^{D}k_{STO}$ at −5 °C and 5 °C (Tables 2 and 3), in agreement with the rate of hydride transfer dominating, albeit not absolutely determining, the rate of conversion of *Ab*HBDH:NADH:3OV to *Ab*HBDH:NAD^+:3HV.

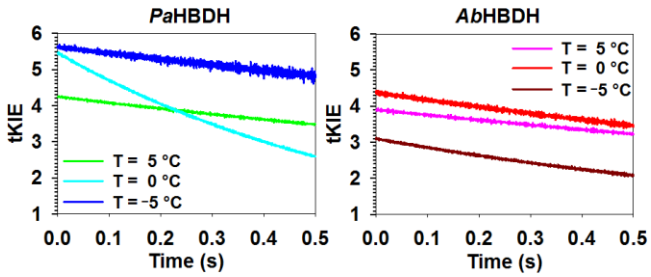

Figure 3. Time-dependent kinetic isotope effects (tKIE) for *Pa*HBDH and *Ab*HBDH at low temperature.

Transition-state analysis of *Pa*HBDH and *Ab*HBDH reactions at 5 °C. Quantum-mechanical tunnelling has been shown to contribute to the rate of several enzyme-catalysed hydride-transfer reactions even when the intrinsic primary deuterium kinetic isotope effect does not exceed the zero-point-energy-derived limit of ~7,[27-30] for instance based on the disruption of presumed coupled-motions due to the lower tunnelling probability of deuterium in comparison with protium in multiple-isotope effects experiments,[30] the breakdown of the Swain-Schaad exponential relationship[31] predicted for semi-classical reaction trajectories involving protium, deuterium, and tritium labelling,[29] the breakdown of the rule of the geometric mean when measuring primary and secondary isotope effects,[28] and the difference

in activation energies and ratio of pre-exponential factors in Arrhenius plots of nonadiabatic reactions involving deuterium-labelled and unlabelled substrates.[32] All of these approaches require either labelling with deuterium and tritium and/or deuteration at multiple positions,[28-30] or that the hydride-step be rate-determining at all experimental temperatures.[32, 33]

Table 3. Intrinsic primary deuterium kinetic isotope effects ($^{D}k_5$) for *Pa*HBDH- and *Ab*HBDH-catalysed reduction of 3-oxovalerate.

	–5 °C	**0 °C**	**5 °C**
***Pa*HBDH $^{D}k_5$**	5.7 ± 0.5	5.5 ± 0.4	4.2 ± 0.3
***Ab*HBDH $^{D}k_5$**	3.1 ± 0.4	4.4 ± 0.2	3.9 ± 0.2

In the *Pa*HBDH and *Ab*HBDH reactions, we assume some contribution from tunnelling, especially at low temperature. However, a quantitative evaluation of this contribution is not possible due to the single-isotope and single-position labelling employed here, and the fact chemistry is not rate-determining at every temperature, as evidenced by $^{D}k_5 > {}^{D}k_{STO}$ in most cases. Thus, we limited our evaluation of $^{D}k_5$ to a semi-classical interpretation of transition-state structures. We recently reported models of the *Pa*HBDH- and *Ab*HBDH-catalysed reduction of 3-oxovalerate based on a "static" QM/MM approach, which captured the concerted nature of hydride- and proton-transfers derived from primary and solvent isotope effects.[15] Theoretical kinetic isotope effects for hydride transfer calculated at 5 °C from those models yielded values of 4.0 ± 0.2 for *Pa*HBDH, in excellent agreement with $^{D}k_5$ at the same temperature, and 3.2 ± 0.1 for *Ab*HBDH, in reasonable agreement with $^{D}k_5$ at 5 °C, suggesting both reactions proceed via late, product-like transition states regarding hydride transfer (Figure 4). In the transition-state models, hydride transfer to C3 of 3-oxovalerate is slightly more advanced in the *Ab*HBDH reaction than in the *Pa*HBDH one, in agreement with the marginally

lower value of *Ab*HBDH $^{D}k_5$ as compared with *Pa*HBDH $^{D}k_5$ at 5 °C.

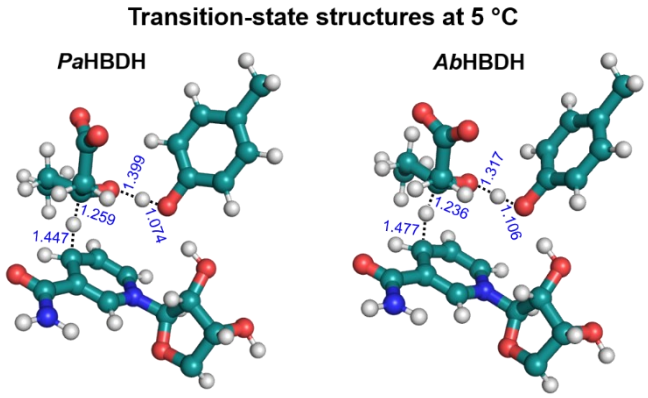

Figure 4. Transition-state models for *Pa*HBDH- and *Ab*HBDH-catalysed reduction of 3-oxovalerate[15] at 5 °C. Only the QM regions are shown. Dashed-lines depict partial bonds, and associated numbers denote mean distances (Å) of 10 replicates optimized at the M06-2X/ma-def2-SVP level of theory. Standard error of the mean distances are shown in Table S4.

Interpretation of transition states of *Pa*HBDH and *Ab*HBDH reactions at –5 °C. Theoretical kinetic isotope effects for hydride transfer calculated at 0 and –5 °C increased monotonically with decreasing temperature (Table S5). While they remained always higher for the psychrophilic than for the mesophilic orthologue, they do not capture the correct temperature dependence of $^{D}k_5$. This discrepancy may result from a combination of factors, for example, from a quantum-mechanical perspective, a larger contribution from tunneling at lower temperatures would be expected, which the one-dimensional Bell infinite parabola model does not correctly describe.[34] Within a semi-classical framework, the change in $^{D}k_5$ reflects a change in the transition-state ensemble geometry at lower temperatures, which is not accurately described by the "static" QM/MM methodology.

Primary deuterium kinetic isotope effects will approach the semi-classical upper limit of ~7 when the transferring particle experiences maximum difference in its bond-order between ground state and transition state.[27] For hydride-transfer reactions, this condition is satisfied by

loose, symmetric transition states, while both early and late, asymmetric transition states will result in comparatively smaller net-change in hydride bonding environment, deflating the isotope effect.[27, 35] At −5 °C, *Pa*HBDH $^{D}k_5$ increases to 5.7, indicating a symmetric or near-symmetric transition-state geometry for hydride transfer (Figure 5). On the other hand, *Ab*HBDH $^{D}k_5$ decreases to 3.1 at −5 °C, pointing to an even more asymmetric, probably product-like transition-state geometry for hydride transfer (Figure 5).

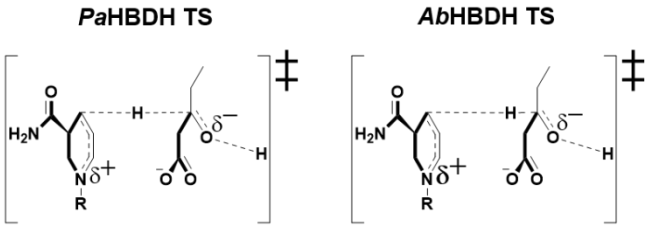

Figure 5. Proposed transition states for *Pa*HBDH and *Ab*HBDH-catalysed hydride transfer at −5 °C. R = ribosyl-diphosphate-adenosine.

The trend $^{D}k_5 > {}^{D}k_{STO} > {}^{D}k_{cat}$ along with the altered transition-state symmetry in *Pa*HBDH catalysis at sub-zero temperature might be involved in the cold-adaptation of this enzyme. However, it is noteworthy that other SDR orthologues can also catalyse hydride transfers to carbonyls with distinct degrees of symmetry at the transition state. For instance, an intrinsic primary deuterium isotope effect of 2.7 for *Streptococcus pneumonia* 3-oxoacyl-ACP reductase, combined with a high α-secondary deuterium isotope effect, established a late transition state for hydride transfer,[36] while an intrinsic primary deuterium isotope effect lower limit of 4.5 for *Mycobacterium tuberculosis* 3-oxoacyl-ACP reductase suggests a relatively more symmetric transition state,[37] and both of these orthologues are mesophilic.

His150Asn-*Pa*HBDH and Asn145His-*Ab*HBDH $^{D}k_{cat}$ at 5 °C. In spite of the their overall low amino acid sequence identity, *Pa*HBDH and *Ab*HBDH have highly conserved active sites, with only one diverging position: His150 in *Pa*HBDH is equivalent to Asn145 in

*Ab*HBDH (Figure 6A).[15] In comparison to the corresponding WT-*Pa*HBDH and WT-*Ab*HBDH, a 52-fold, 4300-fold, 31-fold, and 7-fold decrease in k_{cat} for acetate reduction at 5 °C is observed for His150Ala-*Pa*HBDH, His150Asn-*Pa*HBDH, Asn145Ala-*Ab*HBDH, Asn145His-*Ab*HBDH (Figure 6B and Table S6), indicating that while a *Pa*HBDH-like active site has only modest impact on *Ab*HBDH catalysis, an *Ab*HBDH-like active site drastically disrupts *Pa*HBDH catalysis. This suggests that outer protein shells exert a major influence on *Pa*HBDH catalysis, but only modest influence on *Ab*HBDH catalysis, a similar trend to what was observed at 10 °C,[15] but even more pronounced at 5 °C. Acetoacetate reduction at 0 and –5 °C and reduction of 3-oxovalerate at any temperature could not be accurately measured due to extremely low rates with most of the mutants.

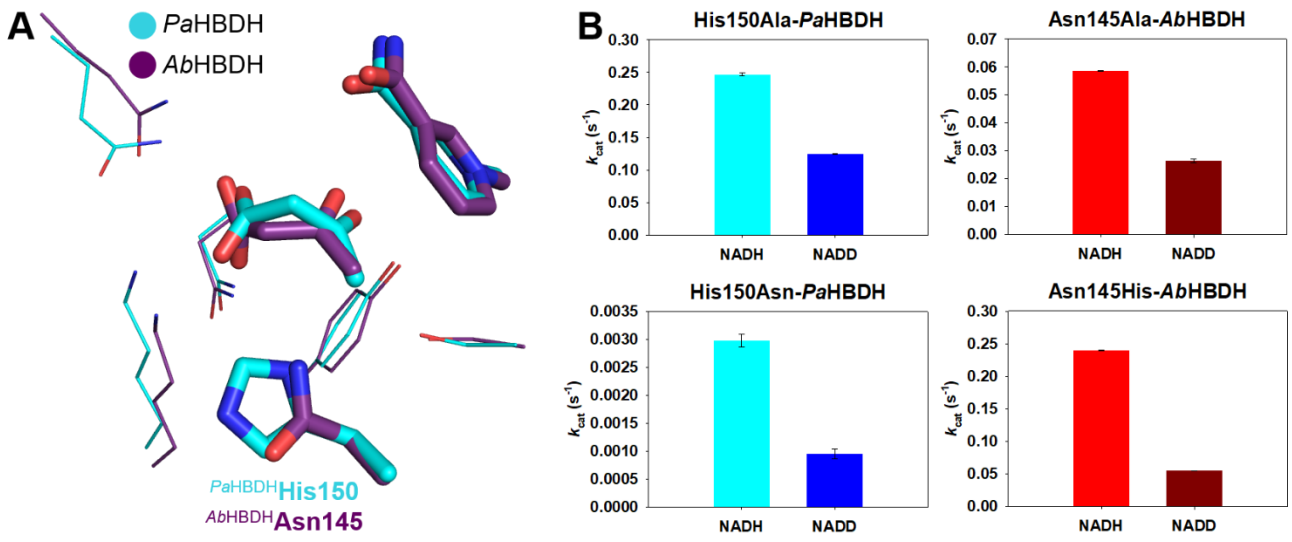

Figure 6. Analysis of *Pa*HBDH and *Ab*HBDH active-site mutations. (A) Overlay of *Pa*HBDH:NAD^+:acetoacetate (PDB ID: 6ZZO) and *Ab*HBDH:NAD^+:acetoacetate (PDB ID: 6ZZQ) active sites.[15] Acetoacetate, nicotinamide moiety of NAD+, and His150/Asn145 side chains are shown as stick, while other residue side chains are shown as wireframe. (B) *Pa*HBDH and *Ab*HBDH mutants k_{cat} for acetoacetate reduction at 5 °C in the presence of either NADH or NADD. Substrates and coenzymes were held at saturating concentrations. Each bar represents mean ± SE of at least 4 replicates for His150Ala-*Pa*HBDH, Asn145Ala-*Ab*HBDH,

and Asn145His-*Ab*HBDH, or triplicates for His150Asn-*Pa*HBDH.

In order to evaluate if the decrease in k_{cat} may be associated with a change in rate-limiting step where hydride transfer becomes more rate-limiting with the mutants, we determined $^{D}k_{cat}$ for all four HBDH mutants (Figure 6B). Hydride transfer is negligibly rate-limiting for acetoacetate reduction by *Pa*HBDH at 5 °C, but partially rate-limiting with *Ab*HBDH at that temperature (Table 1). His150Ala-*Pa*HBDH $^{D}k_{cat}$ equals 1.98 ± 0.02 and Asn145Ala-*Ab*HBDH $^{D}k_{cat}$ equals 2.2 ± 0.1, very similar to the respective $^{D}k_{cat}$ obtained with WT-*Pa*HBDH and WT-*Ab*HBDH, suggesting the significant decreases in rates arising from the alanine substitutions do not reflect an altered contribution of the hydride-transfer step to the overall reaction rate.

His150Asn-*Pa*HBDH $^{D}k_{cat}$ equals 3.1 ± 0.1, representing an increase from the WT-*Pa*HBDH $^{D}k_{cat}$ of 1.7, suggesting the 4300-fold reduction in rate imposed by the asparagine substitution exposes the chemical step. Intriguingly, Asn145His-*Ab*HBDH $^{D}k_{cat}$ equals 4.4 ± 0.1, twice the WT-*Ab*HBDH $^{D}k_{cat}$ even though only a modest decrease in rate is imposed by the histidine substitution. Assuming (*i*) reactions with acetoacetate and 3-oxovalerate proceed via similar transition-state structures and (*ii*) hydride transfer dominates His150Asn-*Pa*HBDH and Asn145His-*Ab*HBDH k_{cat}, comparison of $^{D}k_5$ for the wild-type enzymes with $^{D}k_{cat}$ for His150Asn-*Pa*HBDH and Asn145His-*Ab*HBDH might suggest that introduction of an *Ab*HBDH-like active site into *Pa*HBDH leads to a more asymmetric transition-state geometry for the psychrophilic enzyme reaction, while introduction of a *Pa*HBDH-like active site into *Ab*HBDH increases the transition-state symmetry of the reaction with the mesophilic enzyme. Transition-state structures have been reported to vary even for highly conserved enzyme orthologues. For example, human and bovine purine nucleoside phosphorylase reactions proceed by distinct transition states in spite of sharing 87% overall amino acid sequence

identity and 100% sequence identity in the active site.[38, 39]

In summary, we sought to uncover differences in kinetics of cold- and warm-adapted HBDHs near the temperature where the former evolved to function. We demonstrated that hydride transfer becomes less rate-limiting for the psychrophilic enzyme as the temperature is lowered, while for the mesophilic enzyme, hydride transfer is significantly rate-limiting across the three experimental temperatures. Our results also uncovered differences in transition-state symmetry between *Pa*HBDH and *Ab*HBDH reactions modulated both by temperature and a single diverging position in otherwise highly conserved active sites. In a previous phylogenetic analysis of bacterial HBDHs adapted to various environments, harboring a either a histidine or an asparagine in that diverging position defines two distinct clusters of HBDHs, with both clusters comprising bacteria adapted to all sampled habitats.[15] Hence, further research may help establish whether temperature- and single residue-modulation of transition-state geometry is a general feature of HBDHs, and perhaps of other SDRs.

SUPPORTING INFORMATION AVAILABLE

Further experimental results and theoretical analysis of *Pa*HBDH and *Ab*HBDH catalysis. This material is available free of charge via the internet at http://pubs.acs.org.

ACCESSION CODES

*Pa*HBDH: UniProt Q4FRT2

*Ab*HBDH: UniProt A0A1E3M3N6

ABBREVIATIONS

SDR, short-chain dehydrogenase/reductase; HBDH, (*R*)-3-hydroxyburyrate dehydrogenase; *Pa*HBDH, *P. arcticus* HBDH; *Ab*HBDH, *A. baumannii* HBDH; NADH, reduced nicotinamide-adenine dinucleotide; NAD^+, oxidised nicotinamide-adenine dinucleotide; QM/MM, quantum

mechanics/molecular mechanics; WT, wild-type; k_{cat}, steady-state catalytic constant; k_{STO}, single-turnover rate constant; 3OV, 3-oxovalerate; 3HV, (*R*)-3-hydroxyvalerate.

ACKNOWLEDGMENTS

This work was supported by the Engineering and Physical Sciences Research Council (EPSRC) [grant number EP/L016419/1] via a CRITICAT Centre for Doctoral Training studentship to T.F.G.M., by the Wellcome Trust via an Institutional Strategic Support Fund [grant number 204821/Z/16/Z] to the University of St Andrews, and by the Swedish Research Council and KAW Foundation grants to J.Å.

REFERENCES

[1] Persson, B., and Kallberg, Y. (2013) Classification and nomenclature of the superfamily of short-chain dehydrogenases/reductases (SDRs), *Chem. Biol. Interact. 202*, 111-115.

[2] Kavanagh, K. L., Jornvall, H., Persson, B., and Oppermann, U. (2008) Medium- and short-chain dehydrogenase/reductase gene and protein families: the SDR superfamily: functional and structural diversity within a family of metabolic and regulatory enzymes, *Cell. Mol. Life Sci. 65*, 3895-3906.

[3] Qin, F., Qin, B., Zhang, W., Liu, Y., Su, X., Zhu, T., Ouyang, J., Guo, J., Li, Y., Zhang, F., Tang, J., Jia, X., and You, S. (2018) Discovery of a Switch Between Prelog and Anti-Prelog Reduction toward Halogen-Substituted Acetophenones in Short-Chain Dehydrogenase/Reductases, *ACS Catal. 8*, 6012-6020.

[4] Gong, X.-M., Qin, Z., Li, F.-L., Zeng, B.-B., Zheng, G.-W., and Xu, J.-H. (2018) Development of an Engineered Ketoreductase with Simultaneously Improved Thermostability and Activity for Making a Bulky Atorvastatin Precursor, *ACS Catal. 9*, 147-153.

[5] Bergmeyer, H. U., Gawehn, K., Klotzsch, H., Krebs, H. A., and Williamson, D. H. (1967) Purification and properties of crystalline 3-hydroxybutyrate dehydrogenase from *Rhodopseudomonas spheroides*, *Biochem. J. 102*, 423-431.

[6] Iimori, T., and Shibasaki, M. (1986) Simple, stereocontrolled synthesis of 1β-methylcarbapenem antibiotics from 3(R)-hydroxybutyric acid, *Tetrahedron Let. 27*, 2149-2152.

[7] Tokiwa, Y., and Ugwu, C. U. (2007) Biotechnological production of (R)-3-hydroxybutyric acid monomer, *J. Biotechnol. 132*, 264-272.

[8] Yeon, Y. J., Park, H. Y., and Yoo, Y. J. (2013) Enzymatic reduction of levulinic acid by engineering the substrate specificity of 3-hydroxybutyrate dehydrogenase, *Bioresour. Technol. 134*, 377-380.

[9] Fluchter, S., Follonier, S., Schiel-Bengelsdorf, B., Bengelsdorf, F. R., Zinn, M., and Durre, P. (2019) Anaerobic Production of Poly(3-hydroxybutyrate) and Its Precursor 3-Hydroxybutyrate from Synthesis Gas by Autotrophic Clostridia, *Biomacromolecules 20*, 3271-3282.

[10] Lee, H.-S., Na, J. G., Lee, J., and Yeon, Y. J. (2019) Structure-based Mutational Studies of D-3-hydroxybutyrate Dehydrogenase for Substrate Recognition of Aliphatic Hydroxy Acids with a Variable Length of Carbon Chain, *Biotechnol. Bioproc. Eng. 24, 605-612.*

[11] Machado, T. F. G., Gloster, T. M., and da Silva, R. G. (2018) Linear Eyring Plots Conceal a Change in the Rate-Limiting Step in an Enzyme Reaction, *Biochemistry 57*, 6757-6761.

[12] Ayala-del-Rio, H. L., Chain, P. S., Grzymski, J. J., Ponder, M. A., Ivanova, N., Bergholz, P. W., Di Bartolo, G., Hauser, L., Land, M., Bakermans, C., Rodrigues, D., Klappenbach, J., Zarka, D., Larimer, F., Richardson, P., Murray, A., Thomashow, M.,

and Tiedje, J. M. (2010) The genome sequence of *Psychrobacter arcticus* 273-4, a psychroactive Siberian permafrost bacterium, reveals mechanisms for adaptation to low-temperature growth, *Appl. Environ. Microbiol. 76*, 2304-2312.

[13] Chen, C.-C., Lin, Y.-C., Sheng, W.-H., Chen, Y.-C., Chang, S.-C., Hsia, K.-C., Liao, M.-H., and Li, S.-Y. (2011) Genome Sequence of a Dominant, Multidrug-Resistant *Acinetobacter baumannii* Strain, TCDC-AB0715, *J. Bacteriol. 193*, 2361-2362.

[14] Feller, G., and Gerday, C. (2003) Psychrophilic enzymes: hot topics in cold adaptation, *Nat. Rev. Microbiol. 1*, 200-208.

[15] Machado, T. F. G., Purg, M., McMahon, S. A., Read, B. J., Oehler, V., Åqvist, J., Gloster, T. M., and da Silva, R. G. (2020) Dissecting the Mechanism of (R)-3-Hydroxybutyrate Dehydrogenase by Kinetic Isotope Effects, Protein Crystallography, and Computational Chemistry, *ACS Catal. 10*, 15019-15032.

[16] Palfey, B. A., and Fagan, R. L. (2006) Analysis of the kinetic isotope effects on initial rates in transient kinetics, *Biochemistry 45*, 13631-13640.

[17] Paton, R. (2016) Kinisot: v 1.0.0 public API for Kinisot.py, *Zenodo*.

[18] Kesharwani, M. K., Brauer, B., and Martin, J. M. L. (2015) Frequency and Zero-Point Vibrational Energy Scale Factors for Double-Hybrid Density Functionals (and Other Selected Methods): Can Anharmonic Force Fields Be Avoided?, *J. Phys. Chem. A 119*, 1701-1714.

[19] Johnson, K. A. (1992) 1 Transient-State Kinetic Analysis of Enzyme Reaction Pathways, In *The Enzymes* (Sigman, D. S., Ed.), pp 1-61, Academic Press.

[20] Northrop, D. B. (1975) Steady-state analysis of kinetic isotope effects in enzymic reactions, *Biochemistry 14*, 2644-2651.

[21] Northrop, D. B. (1981) The expression of isotope effects on enzyme-catalyzed reactions, *Annu. Rev. of Biochem. 50*, 103-131.

[22] Cleland, W. W. (1982) The use of isotope effects to determine transition-state structure for enzymic reactions, *Methods Enzymol. 87*, 625-641.

[23] Schramm, V. L. (2011) Enzymatic transition states, transition-state analogs, dynamics, thermodynamics, and lifetimes, *Annu. Rev. of Biochem. 80*, 703-732.

[24] Preuveneers, M. J., Peacock, D., Crook, E. M., Clark, J. B., and Brocklehurst, K. (1973) D-3-hydroxybutyrate dehydrogenase from *Rhodopseudomonas spheroides*. Kinetic mechanism from steady-state kinetics of the reaction catalysed by the enzyme in solution and covalently attached to diethylaminoethylcellulose, *Biochem. J. 133*, 133-157.

[25] Kluger, R., Nakaoka, K., and Tsui, W.-C. (1978) Substrate analog studies of the specificity and catalytic mechanism of D-3-hydroxybutyrate dehydrogenase, *J. Am. Chem. Soc. 100*, 7388-7392.

[26] Maniscalco, S. J., Tally, J. F., and Fisher, H. F. (2004) The interpretation of multiple-step transient-state kinetic isotope effects, *Arch. Biochem. Biophys. 425*, 165-172.

[27] Westheimer, F. H. (1961) The Magnitude of the Primary Kinetic Isotope Effect for Compounds of Hydrogen and Deuterium, *Chem. Rev. 61*, 265-273.

[28] Delgado, M., Görlich, S., Longbotham, J. E., Scrutton, N. S., Hay, S., Moliner, V., and Tuñón, I. (2019) Convergence of theory and experiment on the role of preorganization, quantum tunneling and enzyme motions into flavoenzyme-catalyzed hydride transfer, *ACS Catal. 7*, 3190-3198.

[29] Cha, Y., Murray, C. J., and Klinman, J. P. (1989) Hydrogen tunneling in enzyme reactions, *Science 243*, 1325-1330.

[30] Hermes, J. D., and Cleland, W. W. (1984) Evidence from multiple isotope effect determinations for coupled hydrogen motion and tunneling in the reaction catalyzed by glucose-6-phosphate dehydrogenase, *J. Am. Chem. Soc. 106*, 7263-7264.

[31] Swain, C. G., Stivers, E. C., Reuwer, J. F., and Schaad, L. J. (1958) Use of Hydrogen Isotope Effects to Identify the Attacking Nucleophile in the Enolization of Ketones Catalyzed by Acetic Acid1-3, *J. Am. Chem. Soc. 80*, 5885-5893.

[32] Klinman, J. P., and Offenbacher, A. R. (2018) Understanding Biological Hydrogen Transfer Through the Lens of Temperature Dependent Kinetic Isotope Effects, *Acc. Chem. Res. 51*, 1966-1974.

[33] Johannissen, L. O., Iorgu, A. I., Scrutton, N. S., and Hay, S. (2019) What are the signatures of tunnelling in enzyme-catalysed reactions?, *Faraday Discuss. 221*, 367-378.

[34] Truhlar, D. G., Gao, J., Garcia-Viloca, M., Alhambra, C., Corchado, J., Luz Sanchez, M., and Poulsen, T. D. (2004) Ensemble-averaged variational transition state theory with optimized multidimensional tunneling for enzyme kinetics and other condensed-phase reactions, *Int. J. Quantum Chem. 100*, 1136-1152.

[35] Cook, P. F. (1998) Mechanism from isotope effects, *Isotopes Environ. Health Stud. 34*, 3-17.

[36] Patel, M. P., Liu, W. S., West, J., Tew, D., Meek, T. D., and Thrall, S. H. (2005) Kinetic and chemical mechanisms of the fabG-encoded *Streptococcus pneumoniae* beta-ketoacyl-ACP reductase, *Biochemistry 44*, 16753-16765.

[37] Silva, R. G., de Carvalho, L. P., Blanchard, J. S., Santos, D. S., and Basso, L. A. (2006) *Mycobacterium tuberculosis* beta-ketoacyl-acyl carrier protein (ACP) reductase: kinetic and chemical mechanisms, *Biochemistry 45*, 13064-13073.

[38] Lewandowicz, A., and Schramm, V. L. (2004) Transition state analysis for human and *Plasmodium falciparum* purine nucleoside phosphorylases, *Biochemistry 43*, 1458-1468.

[39] Kline, P. C., and Schramm, V. L. (1993) Purine nucleoside phosphorylase. Catalytic mechanism and transition-state analysis of the arsenolysis reaction, *Biochemistry 32*, 13212-13219.

“For Table for Contents use only”